

Title:**Machine Learning-Based Reward-Driven Tuning of Scanning Probe Microscopy: Towards Fully Automated Microscopy****Authors:**

Yu Liu^{1*}, Roger Proksch^{1,2}, Jason Bemis², Utkarsh Pratiush¹, Astita Dubey^{1,5}, Mahshid Ahmadi¹, Reece Emery¹, Philip D. Rack¹, Yu-Chen Liu⁴, Jan-Chi Yang⁴, Sergei V. Kalinin^{1,3*}

¹ Institute for Advanced Materials and Manufacturing, Department of Materials Science and Engineering, University of Tennessee, Knoxville, Tennessee, 37996 USA

² Oxford Instruments Asylum Research, Santa Barbara, California 93117, USA

³ Physical Sciences Division, Pacific Northwest National Laboratory, Richland, WA 99354

⁴ Department of Physics, National Cheng Kung University, Tainan 70101, Taiwan

⁵ Institute for Materials Science and Center for Nanointegration Duisburg-Essen (CENIDE), University of Duisburg-Essen, Universitätsstr. 15, 45141 Essen, Germany

* Corresponding author: yliu206@utk.edu, sergei2@utk.edu

Abstract

Since the dawn of scanning probe microscopy (SPM), tapping or intermittent contact mode has been one of the most widely used imaging modes. Manual optimization of tapping mode not only takes a lot of instrument and operator time, but also often leads to frequent probe and sample damage, poor image quality and reproducibility issues for new types of samples or inexperienced users. Despite wide use, optimization of tapping mode imaging is an extremely hard problem, ill-suited to either classical control methods or machine learning. Here we introduce a reward-driven workflow to automate the optimization of SPM in the tapping mode. The reward function is defined based on multiple channels with physical and empirical knowledge of good scans encoded, representing a sample-agnostic measure of image quality and imitating the decision-making logic employed by human operators. This automated workflow gives optimal scanning parameters for different probes and samples and gives high-quality SPM images consistently in the attractive mode. This study broadens the application and accessibility of SPM and opens the door for fully automated SPM.

Introduction

Scanning probe microscopy (SPM) has revolutionized our understanding of the nanoworld, providing unprecedented insights into the structure and properties of materials at the nanoscale. This powerful technique allows for structural imaging in diverse environments, including ambient conditions, liquids, and vacuum, making it versatile for various applications [1-3]. Over the years, SPM has evolved significantly, building upon the initial contact and non-contact modes [4, 5] to yield a broad array of advanced imaging modes. These advancements have been driven by continuous improvements in hardware and electronics, culminating in the ability to achieve atomic resolution imaging even in ambient conditions [6].

Topographic imaging in SPM not only reveals the surface morphology but also provides additional information through various signal channels. For instance, in the basic tapping mode with periodic drive, phase signals can be obtained and offer insights into material properties and interactions [7, 8]. Moreover, SPM's versatility is further enhanced by the introduction of multi-frequency modes, as demonstrated in [9, 10]. These modes enable the simultaneous acquisition of multiple data channels, enriching our understanding of the sample's properties.

The range of functional imaging modes available in SPM is broad and encompasses various physical properties, such as magnetic [5, 11, 12], mechanical [4, 5], biological [3, 13-15], ferroelectric [16], and electrical characteristics [5, 17]. Each of these modes allows researchers to probe different aspects of the sample, providing a comprehensive view of its functional behavior. However, the effectiveness and reliability of these functional imaging modes are critically dependent on the quality of topographic imaging. Operators must simultaneously achieve multiple objectives, including optimizing image stability, enhancing resolution, and minimizing both reversible and irreversible changes in the probe and sample states. Achieving these goals is a complex and time-consuming process that requires significant expertise. The success of SPM imaging heavily depends on the operator's skill and experience, often leading to irreproducible results when different operators or probes are involved. For example, when imaging hard samples like crystals and ceramics [3, 18-20], a set of inappropriate scanning parameters can lead to fast probe degradation and poor image quality. On soft samples such as soft matters and liquid samples [2, 14, 15, 21-23], non-optimal scanning parameters lead to irreversible sample damage and poor image quality. This challenge is particularly pronounced when dealing with soft systems, nanoparticles, molecules, high-resolution imaging, and imaging in liquids. Transitioning from robust calibration on hard samples to these more delicate and complex systems requires meticulous optimization.

One of the most widely used SPM imaging modes is tapping mode [24, 25], also known as intermittent contact (AC) or amplitude-modulated (AM) mode. In tapping mode, the cantilever is driven at or near its lowest resonance frequency. The amplitude and phase of its oscillations are detected using a lock-in amplifier. As the tip approaches the surface, the tip-surface interactions dampen the cantilever's amplitude, which can then be used as a feedback signal for topographic imaging. A key advantage of tapping mode is its ability to significantly

reduce tip and surface damage, making it suitable for imaging much softer samples compared to contact mode.

Optimizing the scanning parameters in tapping mode is a very difficult task. This is ill-suited to machine learning methods, as all surfaces are different and hence the classical supervised ML paradigm is poorly applicable [26]. This problem is equally complex for classical control methods, as it is not clear how the cantilever dynamics translate into image quality. Each sample's unique topography, mechanical properties, and environmental interactions contribute to a complex, high-dimensional parameter space that defies straightforward modeling or control. Traditional approaches struggle with this variability, often resulting in suboptimal imaging conditions that can lead to poor resolution, increased noise, or even damage to the sample and the probe [27, 28]. At the same time, we note that human operators learn to optimize the scanning conditions, and this knowledge is transferable between different materials and instruments. Skilled operators can intuitively adjust parameters based on their knowledge and experience, achieving high-quality imaging through iterative experimentation and fine-tuning. Hence, we seek to develop an approach that allows transferring the human operator decision-making principles to machine learning workflows. By incorporating human expertise into a reward-driven machine learning framework, we aim to automate the optimization process, ensuring consistent, high-quality imaging across diverse samples and conditions, while reducing the dependency on operator expertise and minimizing the risk of errors.

In this work, we demonstrate that reward-driven, rather than data-driven, machine learning methods can effectively automate the optimization of SPM imaging for various samples, probes, and microscopes in a traceable manner with minimal requirement of computation power that can be fulfilled on a local computer without use of graphic processing unit (GPU), which makes it widely accessible. The key innovation in our approach is the introduction of a reward function that transforms the tuning problem into a classical optimization task. This reward function is based on the trace and retrace scan lines of height and phase channels, incorporating both physical and empirical knowledge of high-quality scans. Essentially, the reward function emulates human expertise, guiding the machine learning algorithm to optimize imaging parameters and consistently achieve the best possible image quality. Despite its apparent simplicity, this solution has eluded the microscopy community for four decades. By leveraging machine learning, we aim to standardize and streamline the optimization process, reducing dependency on operator expertise and improving the reproducibility of SPM imaging.

Reward function-based optimization

The key aspect of any microscopy experiment is the optimization of image conditions, which typically represents a considerable fraction of the instrument time and effort of the human operator. During this process, the operator tunes the parameters while simultaneously assessing the quality of the data streaming from the instrument. This tuning of imaging conditions in any microscopy mode can be generally represented as an optimization problem within the parameter

space of the instrument controls, which are typically well known and provided by the manufacturer. However, defining image quality presents a very complex problem. For atomically resolved imaging in electron microscopy [29] or scanning tunneling microscopy [30], the shape of atomic columns or the presence and intensity of lattice peaks in Fourier transforms offer natural optimization targets [31]. With the optimization target and parameter space defined, this becomes a classical optimization problem.

In non-atomically resolved imaging, unambiguous measures of image resolution or quality are absent. Furthermore, these cannot be defined using classical machine learning approaches since each topographic image is different and hence unique with respect to previous examples. While supervised ML workflows can be built for mature fields such as semiconductor imaging, this paradigm is limited for open-ended research problems. Additionally, descriptive statistics-based measures tend not to be robust with respect to noise and scan instabilities. Previous attempts at automatically tuning SPM have focused on adjusting the PI (proportional-integral) feedback parameters by defining reward functions based on the alignment of the trace and retrace of the height channel. However, these approaches usually result in scanning parameters that lead to rapid probe and sample degradation.

Despite these challenges, human operators learn to optimize scanning conditions through experience acquired on different samples. They intuitively adjust parameters based on real-time feedback from the instrument and their accumulated knowledge of how different settings affect image quality. This ability to adapt and fine-tune parameters through iterative experimentation enables skilled operators to achieve high-quality imaging even under varying and challenging conditions.

Therefore, the key challenge in automating the optimization of the tapping mode (TM) is to find a reward function that works universally across different probes, materials, topologies, and operational environments. Here we design such a reward function based on trace and retrace scan lines that incorporates both physics-based knowledge and empirical insights. Compared to reward functions defined based on entire images, those based on scan lines are approximately 100 times faster, depending on the number of pixels in the scan. This significant speed advantage makes the optimization process practical for real-time operation. By focusing on the critical features of scan lines, such as the alignment and consistency between trace and retrace lines, we aim to develop a robust and efficient optimization framework that can consistently yield high-quality imaging across a wide range of conditions.

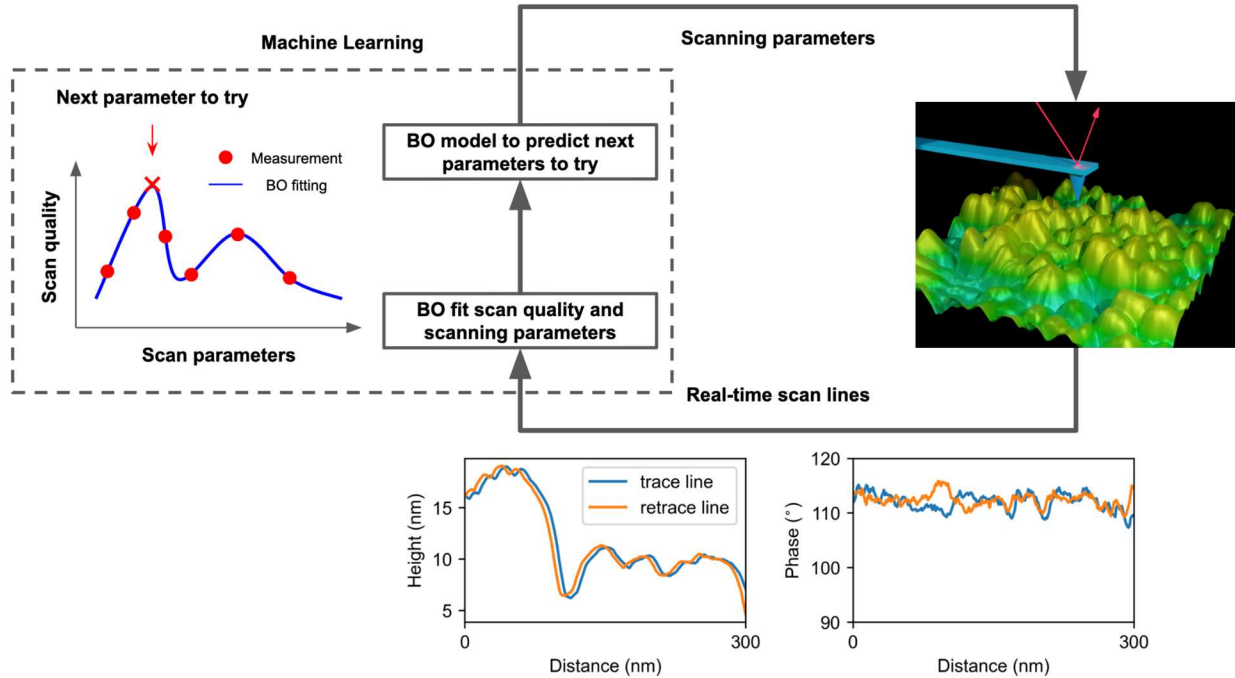


Figure 1. Workflow of optimizing an autonomous microscope.—In the autonomous microscope presented here, we define a reward function to quantify the scan quality. During the Bayesian optimization (BO) process, a Gaussian process (GP) model of reward function is fitted for the explored parameters. This GP model is used to predict the distribution and uncertainty of the reward function in the whole parameter space, from which the next set of parameters will be determined. This iteration process is repeated until the maximum number of optimization steps is reached or the image quality is satisfactory. Thus the machine learning algorithm replaces human operation.

Imaging regimes for TM AFM

Depending on probe types, samples, and setup parameters, SPM can operate in either attractive or repulsive mode [8]. In attractive mode, the microscope tip operates predominantly under long-range attractive forces, such as van der Waals (vdW) interactions, without physical contact. This allows high-resolution imaging while minimizing deformation and damage of probes and samples. Conditions that favor attractive mode include small amplitudes, larger and less sharp tips, and slower but more sensitive and higher quality factors. Probes often transition from repulsive to mixed to attractive mode as they wear and the balance of vdW and adhesive forces changes. This mode excels in achieving high resolution, preserving the integrity of delicate materials like biomolecules [32], and is ideal for imaging soft or loosely bound materials. However, it requires precise control of the tip-sample distance, necessitating meticulous calibration and stability. In the operation of SPM, attractive mode is usually characterized by phases above the free-air phase, which is the measured phase when the probe is very far away from the sample surface.

In contrast, large amplitudes, sharp tips and lower quality factors favor a net-repulsive interaction - where strong, short range repulsive forces dominate. In repulsive mode, the tip intermittently contacts the sample surface, resulting in predominantly short-range repulsive forces, including mechanical contact and repulsive vdW forces [8]. This mode provides enhanced sensitivity for measuring mechanical properties, such as stiffness and viscoelasticity, and offers better contrast, making it easier to distinguish different materials or features. However, the physical contact can lead to sample and probe deformation or damage, reducing image resolution and potentially causing irreversible changes to the probe and sample. While repulsive mode is advantageous for mechanical property measurements, it comes with the trade-off of potential sample alteration and reduced resolution. SPM is operated in the repulsive mode when the measured phases are below the free-air phase.

Because of the tip-shape dependence discussed above, if a probe is initially imaging in repulsive mode, it will often transition from repulsive to mixed to attractive mode as they wear and the balance of vdW and adhesive forces changes. The transition between attractive and repulsive modes can result in high transitory forces [33] and is indicated by phases jumping across the free-air phase.

In this work, we focus on optimizing tip wear while still obtaining high spatial resolution. This requires a stable and robust approach to parameter tuning that can adapt to the varying conditions of different samples and imaging modes. Our goal is to develop a method that ensures consistent high-quality imaging across diverse applications, minimizing the trade-offs between resolution, sensitivity, and sample integrity. By leveraging a reward-driven machine learning framework, we aim to emulate the adaptive expertise of human operators, providing a scalable solution to the complex optimization problem in SPM imaging. This approach promises to enhance the efficiency, reliability and autonomy of SPM, making it more accessible and effective for a wide range of scientific and industrial applications.

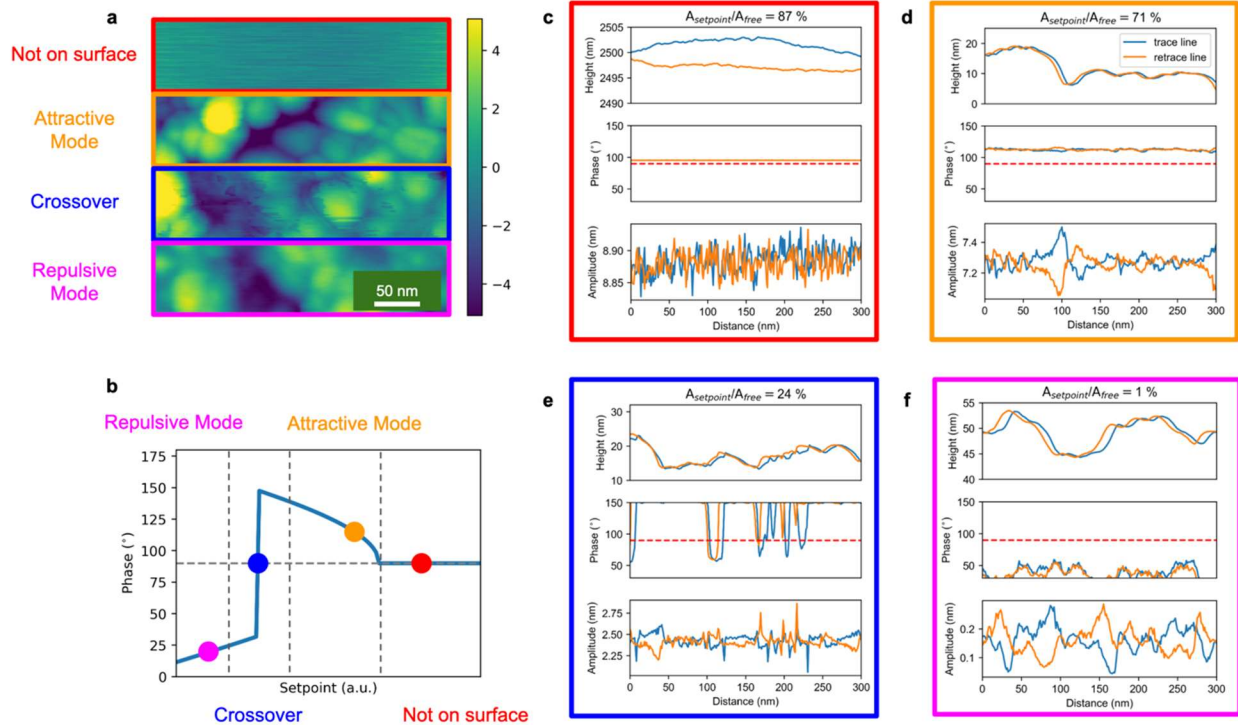


Figure 2. Define reward function to quantify the image quality. **a**, Topography map of TiO_2 nanoparticles shows the effect of scanning parameters on the image quality. In the scan, the free-air amplitude is kept at 10.26 nm and the setpoint amplitude is changed in the middle of the scan. **b**, Schematic plot of the dependence of phase on the setpoint at a fixed free-air amplitude. **c**, Scan trace and retrace lines for a large setpoint. When the setpoint is large, the probe is far away from the sample surface and thus dominated by the long-range probe sample interactions. Consequently, the probe follows the profile of this long-range interaction instead of following the sample surface profile closely. **d**, Trace and retrace lines in the attractive mode. In this mode, the system is dominated by net-attractive interactions between probe and sample, which gives high spatial resolution, phase values above 90-degree, and small dissipation that minimizes probe and sample damage. In this study, we are optimizing this imaging mode. **e**, Trace and retrace lines in the attractive-repulsive crossover mode. As the setpoint is lowered, the system alternates between attractive and repulsive modes. This is indicated by the phase traces jumping above and below the 90-degree line and the presence of probe and sample damage. **f**, Trace and retrace lines in repulsive mode. When the setpoint is small, the probes are in the fully repulsive mode. In this mode, there is a high risk of probe and sample damage.

Define the parameter space and reward function

Below we discuss the relationship between different SPM modes, scan quality, safety of the sample and probe, and the tip-sample distance. In SPM, the tip-sample distance is controlled by the ratio between the setpoint amplitude (A_{setpoint}) and free-air amplitude (A_{drive}),

also known as free amplitude) so the discussion of the physical mechanisms will be guided by the ratio of setpoint amplitude and free-air amplitude.

When the tip is far away from the sample surface (large $A_{\text{setpoint}}/A_{\text{drive}}$), there are no forces between tip and sample. Consequently, the probe is oscillating far above the sample surface instead of following the surface profile, leading to phases close to the free-air phase and random height traces as shown in Figure 2c, subjected to either small drift or other noise in the signal.

As the tip gets closer to the sample surface (smaller $A_{\text{setpoint}}/A_{\text{drive}}$), SPM works in the attractive mode and there are typically long-range attractive forces arising between the tip and surface. This attractive force will decrease the amplitude of the cantilever to the setpoint amplitude at a fixed tip-sample distance, as shown in Figure 2d. As a result, the trace and retrace lines follow closely the sample surface profile with reasonably high spatial resolution and the phases are above the free-air phase. In addition, the force between the tip and sample is kept at a small, net-attractive value and that helps minimize tip and sample damage. This mode is the goal for this work.

When the tip gets even closer to the sample surface (smaller $A_{\text{setpoint}}/A_{\text{drive}}$), SPM jumps between attractive mode and repulsive mode as the interaction between the tip and sample jumps between the long-range attractive forces and short-range repulsive forces. Consequently, there are sudden jumps in the phase traces across the free-air phase in this crossover mode, as shown in Figure 2b. A previous study showed that the transition between attractive and repulsive mode can result in very high transitory forces between the tip and the sample [33]. As a result, the trace and retrace lines match poorly due to the high transitory forces when the phase jumps occur in Figure 2e.

When $A_{\text{setpoint}}/A_{\text{drive}}$ is further decreased, the interaction between the tip and sample is more likely to be completely dominated by the short-range repulsive forces. In this mode, the phases are below the free-air phase most of time. The spatial resolution is suppressed and the tip wears off quickly due to the large forces between the tip and sample, as shown in Figure 2f.

Based on the basic physical principles of SPM discussed above, we define the reward function based on four components derived from the trace and retrace scan lines of the height and phase channels. The height alignment term quantifies the agreement between the trace and retrace lines in the height channel. The phase term measures if the probe is operating in the attractive mode by detecting the presence of phase angles below the free-air phase. The distance term favors lower probe heights to make sure the probe is as close to the sample surface as possible. Finally, the contrast term tries to maximize the amount of information acquired by favoring a large contrast in the height channels. Assembling all these components together, we define the reward function based on a pair of trace and retrace lines of height and phase channels as following equation:

$$\text{Rewards} = -\log(|h_{\text{trace}} - h_{\text{retrace}}|) \times \log(N_{\theta < \theta_{\text{free}}} / N_{\theta > \theta_{\text{free}}}) \times \log(h_{\text{min}} - h_{\text{global min}}) + \log(\sigma_{\text{traces}}) \quad (1)$$

where h_{trace} and $h_{retrace}$ are the trace and retrace height scan lines, $N_{\theta < \theta_{free}}$ and $N_{\theta > \theta_{free}}$ are the number of pixels in the phase scan lines below (repulsive mode) and above (attractive mode) the free phase angles, h_{min} is the lowest probe position of current trace and retrace height lines while $h_{global\ min}$ is the global lowest probe position computed based on all the acquired scan lines, σ_{traces} is the standard deviation of the height lines to represent the contrast.

When the probe is far away from the sample surface and only very weakly interacting with the sample, the traces will be dominated by cantilever sensor noise. Sensor noise will generally have little or no correlation between trace and retrace. The resulting height traces agree poorly with each other and the distance between the probe and sample is large as shown in Figure 2c. Therefore, both the height alignment term and distance term give bad reward values to signal a bad scan. In the attractive mode, every component in our reward function gives good rewards as the height traces align well, the phases are consistently above the free-air phase, the probe is close to the sample surface, and there is a reasonable amount of contrast, as shown in Figure 2d. In the crossover mode as shown in Figure 2e, the phases below the free-air phase leads to a bad reward in the phase term. In the repulsive mode as shown in Figure 2f, most of the pixels in the scan lines show phases below the free-air phase, giving a very small reward to prevent the SPM from working in this mode.

In summary, our proposed reward function accurately distinguishes between a set of good topography scanning parameters in the attractive mode from bad parameters in other modes. In addition, it also leaves the flexibility to adjust the weight of different components to fine-tune for different applications.

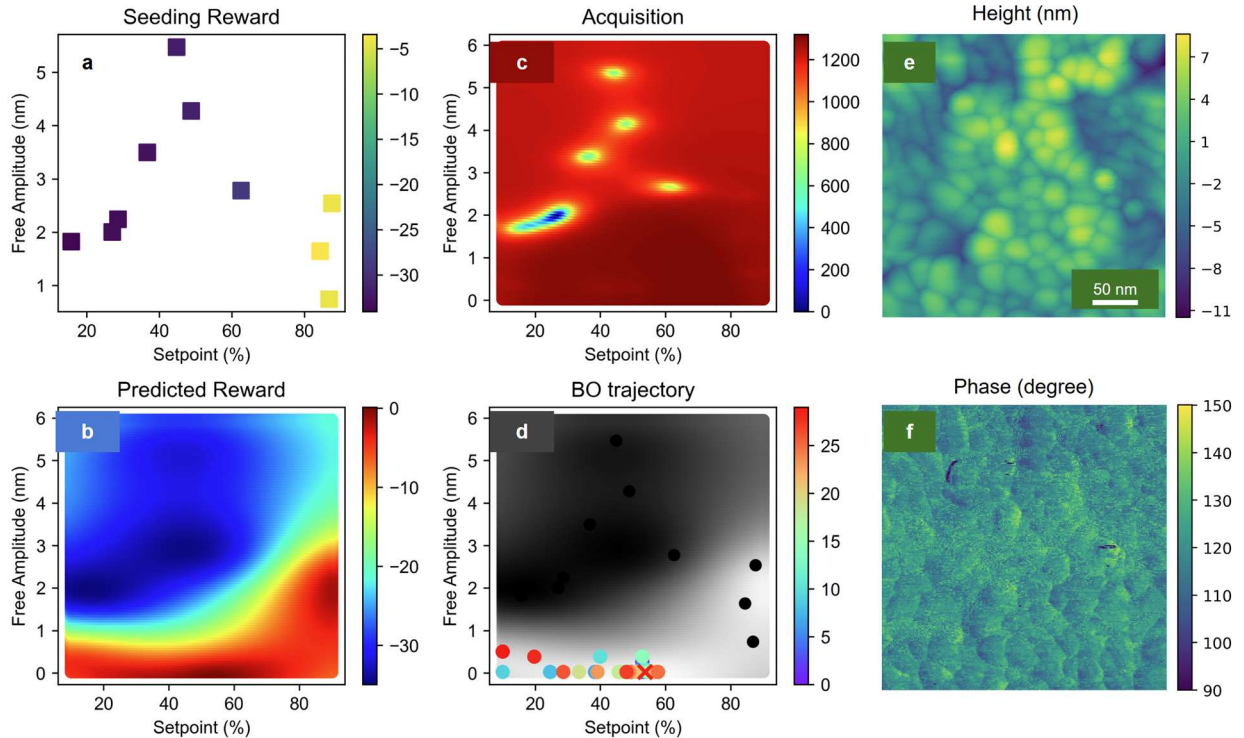


Figure 3. Autonomous tuning of SPM with BO on TiO₂ nanoparticles. **a**, Initial seeding of 10 points and their reward values. **b**, Predicted distribution of reward function in the full parameter space after 30 BO exploration steps. **c**, Acquisition function of log expected improvement (EI). This is computed based on the prediction and uncertainty of the reward function shown in **b** and is used to determine which combination of parameters to measure for the next iteration. **d**, Bayesian optimization trajectory of the seeding and exploration. The optimized scanning parameters are marked by a red cross. **e**, Topography map of TiO₂ nanoparticles taken with the optimized scanning parameters in **d**. **f**, Phase map taken together with **e** shows the full image is taken in the attractive mode.

Reward based optimization and results

We employed Bayesian optimization (BO) to optimize the scanning parameters, focusing on two key parameters: free-air amplitude and setpoint, under consistent conditions. In addition to the physical knowledge about SPM that we encoded into the reward function, we found it necessary to guide the optimization process with human empirical knowledge, especially on defining the parameter space.

To set up a high-resolution scan in the attractive mode, human operators usually start with a small driving voltage and a large setpoint that ensures gentle force between the probe and sample. The smallest free amplitude can be estimated by the roughness of the sample in the given scan size. Then the setpoint is decreased from a large starting value until the trace and retrace lines agree with each other and thus follow the corrugation of the sample surface. Once the free-air amplitude and setpoint are determined, human operators can also increase the integral gain (I gain) as high as possible without the PI loop becoming unstable and oscillatory.

Initially, we defined the parameter space based on the type of probe and the estimated roughness of the sample in the given scan size. For instance, with the Tap300G probe and TiO₂ nanoparticles, the free-air amplitude was constrained between 0.15 nm and 5.9 nm, and the setpoint ranged between 10% and 90% of the free-air amplitude.

Once the parameter space was established, we randomly sampled 10 points within this space to serve as the initial seeding points. The microscope was then controlled via code to measure the scan lines at these parameters, from which the reward function could be computed, as illustrated in Figure 3a. Using the reward values from these seeding points, we fitted an initial Gaussian process (GP) model. This model predicted the distribution and uncertainty of the reward function across the entire parameter space. Subsequently, the acquisition of expected improvement (EI) was computed based on these predictions and uncertainties as shown in Figure 3b-c, determining the next set of parameters to be measured by maximizing the EI acquisition function.

To account for human empirical knowledge of starting the optimization with small free-air amplitude and large setpoint, we masked the acquisition function in the parameter space to enhance the preference on the parameters with smaller free-air amplitude and larger setpoint, as shown in Figure 4c. The scanning parameters were then updated to the new set without interrupting the scan. The reward value for these new parameters was calculated from the newly

acquired trace and retrace scan lines. This new parameters-reward pair was added to the previously collected data to retrain and update the GP model. This iterating process of measuring and fitting was repeated until the maximum number of exploration steps was reached or the scan quality became satisfactory.

Finally, the optimized parameters were used to conduct a full scan to ensure they produced a high-quality image for the entire scan area. As demonstrated in Figures 3e-f, the optimized scanning parameters, determined after 10 seeding steps and 30 exploration steps, yielded high-resolution images with stable operation in the attractive mode. In addition, because the scanning parameters were updated in a non-interruption manner, the optimization was finished within the time of two scans.

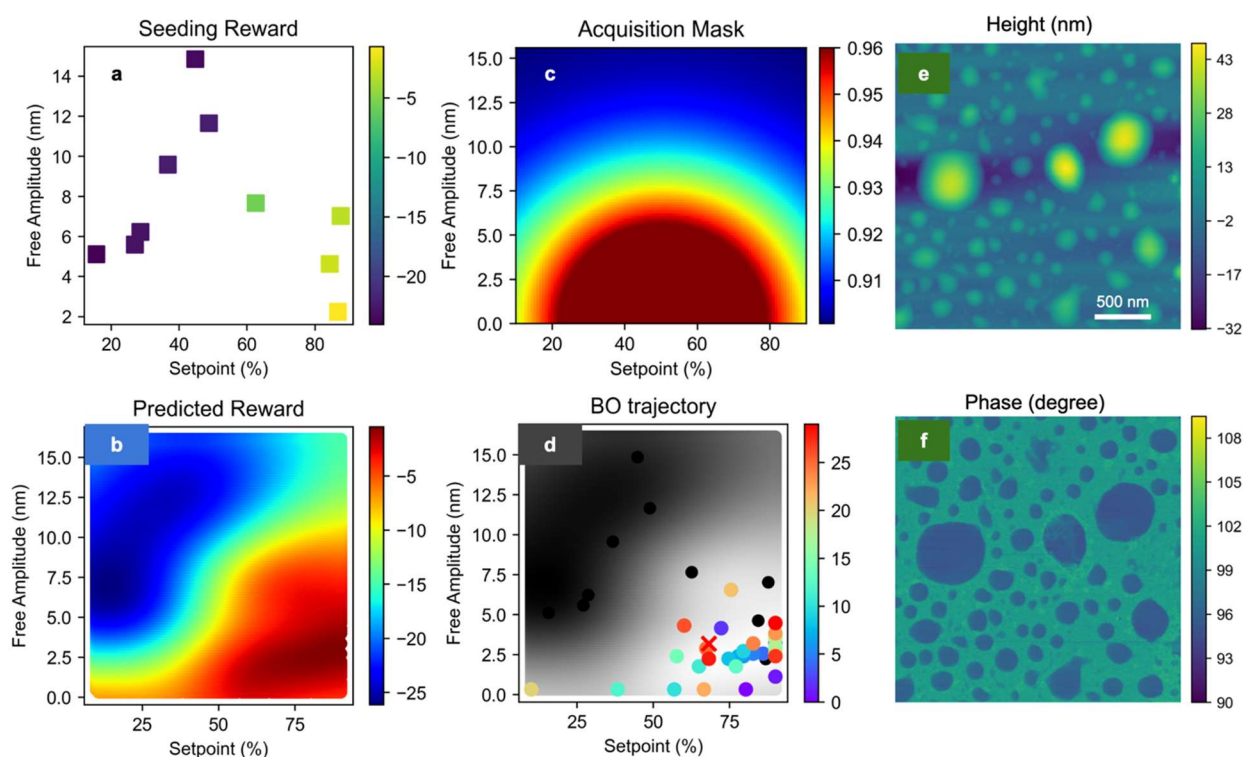


Figure 4. Optimization for more challenging materials: water droplet. **a**, Initial seeding of 10 points and their reward values. **b**, predicted distribution of reward function in the full parameter space after 30 BO exploration steps. **c**, Acquisition mask for guiding the optimization process with human empirical knowledge. By multiplying the EI acquisition function with this acquisition mask, the parameters with lower free-air amplitude and larger setpoint are preferred for the next iteration. **d**, Bayesian optimization trajectory of the seeding and exploration (see Figure S1 for the detailed optimization data associated with the BO trajectory). The optimized scanning parameters are marked by a red cross. **e**, Topography map of water droplet (with CaCl_2 salt saturated solvents) taken with the optimized scanning parameters in **d**. **f**, Phase map taken together with **e** shows the full image is taken in the attractive mode.

More challenging samples – water droplets

After verifying the functionality of our reward-driven optimization workflow on the TiO₂ nanoparticles, we switched to a water droplet sample to challenge our reward-driven workflow. The water droplet on a mica substrate serves as an excellent testing sample for our autonomous optimization workflow. First, the image quality of water droplets is highly sensitive to the tip-sample distance. If the distance is too large, the probe cannot accurately follow the height profile of droplets. Conversely, if the tip-sample distance is too small, a liquid bridge forms between the tip and the droplet, resulting in distortions in the image. More importantly, tuning the scanning parameters for water droplets is challenging even for experienced SPM operators, as the optimal setpoint amplitude and free-air amplitude are confined to a narrow region in the parameter space.

Despite these challenges, we were able to find the optimal scanning parameters that give high-quality TM scans of water droplets with our autonomous workflow as shown in Figure 4e-f. The sharp images of small droplets indicate a high spatial resolution in the image. The smooth image of the large droplets in the height map together with the phase map above the free-phase reveals that the probe works in the net-attractive mode across the whole image and closely follows the height profile of the droplets without distortion.

Conclusion

Our reward-driven automatic optimization of SPM in tapping mode represents a significant advancement for the SPM community. This method not only drastically reduces the instrument time required to tune different probes on various samples but also ensures the acquisition of high-quality and highly reproducible SPM images. This automation increases the application and accessibility of SPM by eliminating the need for extensive manual tuning. Our study lays the groundwork for automating more complex SPM tasks, such as automating more advanced imaging modes and achieving atomic resolution in ambient environments.

Moreover, the broader applicability of this reward-driven optimization workflow across the microscopy community has the potential to transform traditionally complex human-led tasks into streamlined, machine learning-based optimization processes. This shift is crucial for the further automation of microscopy, addressing one of the last significant barriers to fully automated microscopes.

Finally, we anticipate that our workflow will have a profound impact on open science in microscopy. While sharing microscope data alone has provided limited benefits due to the diversity of tasks and applications, the sharing of reward functions introduces a new paradigm. This approach fosters a more integrated and collaborative community, enhancing the reproducibility and efficiency of microscopy research.

This comprehensive solution not only democratizes access to high-quality SPM imaging but also propels the field towards a future where automated, intelligent systems are the norm, significantly advancing both research and industrial applications.

Methods

Technical settings

For the implementation in this paper, we made it light enough to run on a local computer with central process unit (CPU) only. Optimization of scanning parameters in the tapping mode requires an interface library to directly control the SPM and availability of sufficiently high computational power to support the optimization algorithms. Previously, we have developed a Python interface library to control the automation of a Jupiter SPM system manufactured by Oxford Instrument Asylum Research from a local computer without GPU. Connection with HPC will allow more complicated optimization scheme and we have solutions for that [34]. This library not only enables operating the SPM system remotely with code the same way as human operators, but it also has access to the intermediate data like trace and retrace scan lines in all the channels.

Samples

The $(\text{CrVTaW})_x\text{Mo}_{1-x}$ thin film was grown via dc magnetron co-sputtering from a 50 mm diameter Mo and an equiatomic CrVTaW target at 500°C substrate temperature. The system was pumped to $\sim 3 \times 10^{-7}$ Torr and backfilled with Ar to 5 mTorr and the sputtering powers (200 W for CrVTaW and 100 W for Mo) were adjusted to give approximately equivalent sputtering rates (10 nm/min determined via x-ray reflectance) of the two targets at the substrate center. The pseudo binary $(\text{CrVTaW})_x\text{Mo}_{1-x}$ composition varies from 15 x 88 at. % across the 100 mm diameter substrate with a roughly linear composition gradient.

The PbTiO_3 (PTO) thin films were grown on $\text{La}_{0.7}\text{Sr}_{0.3}\text{MnO}_3$ (LSMO) buffered (110)-oriented SrTiO_3 (STO) single crystal substrates using pulsed laser deposition (PLD) with a KrF excimer laser ($\lambda = 248$ nm). The LSMO/PTO layers were deposited at temperatures of 700 °C/690 °C with oxygen pressures of 100 mtorr/150 mtorr, respectively. After deposition, the samples were cooled to room temperature under an oxygen pressure of 700 Torr. The thicknesses of the PTO and LSMO layers are approximately 150 nm and 30 nm, respectively.

$\text{Pb}_{0.995}(\text{Zr}_{0.45}\text{Ti}_{0.55})_{0.99}\text{Nb}_{0.01}\text{O}_3$ films were grown by pulsed laser deposition using a KrF excimer laser from a ceramic target onto a SrRuO_3 -electroded (001) SrTiO_3 single crystal. The SrRuO_3 film was grown from a target from Kojundo Chemical Lab. Co. Ltd., using a laser energy density of 1.5 J/cm², a substrate temperature of 660°C, an oxygen pressure of 120 mTorr, a target-to-substrate distance of 6.7 mm, and a frequency of 5 Hz. The SrRuO_3 film thickness was around 50 nm. The PZT film was grown from a target with 20% excess PbO to compensate for lead loss during growth, using a laser energy density of 1.5 J/cm², a substrate temperature of 630°C, an oxygen pressure of 120 mTorr, a target-to-substrate distance of 6.2 mm, and a frequency of 5 Hz. The PZT film thickness was around 147 nm.

TiO_2 NPs were synthesized via a modified solvothermal method. Titanium tetraisopropoxide (TTIP, 99.95%, Sigma Aldrich) served as the titanium precursor, and anhydrous ethanol was utilized as the solvent. In a standard synthesis, 0.1 M of TTIP was combined with 50 mL of

ethanol and stirred uniformly for one hour. Subsequently, a mixture of 50 mL ethanol and deionized water in a 1:1 ratio was added to the solution, followed by vigorous stirring for another hour. To induce rapid hydrolysis, a few drops of pH 4.0 H₂SO₄ were introduced. The resulting white solution was then placed in a tightly sealed reagent bottle and subjected to solvothermal growth at 90°C for 12 hours. The final products were centrifuged and washed several times with de-ionized water to eliminate any bound sulfate ions. The resulting NPs were dried and annealed at varying temperatures (400 °C) for one hour. These obtained NPs were characterized by X-ray diffraction and scanning electron microscopy for their structure evaluation.

The Cs₃Bi₂I₉ (CBI) microcrystals (MCs) were synthesized through a solvent-free mechanochemical activation method, as detailed elsewhere [35]. In this procedure, the precursors cesium iodide (CsI; Aldrich, 99.999% ultra-dry, metals basis), bismuth iodide (BiI₃; Sigma-Aldrich, 98%), were ground for 15 minutes under ambient conditions using a mortar-pestle. The resultant powder was then washed three times with a mixture of dimethyl formamide (DMF) and dimethyl sulfoxide (DMSO) solution. Afterwards chloroform (CHCl₃) was utilized as an antisolvent to obtain orange microcrystals. The MCs were characterized by X-ray diffraction and scanning electron microscopy for their structure evaluation.

The preparation of CaCl₂-solution droplets on mica substrate follows the recipe described in [22].

SPM setup

All the tapping mode SPM measurements were performed on a Jupiter SPM system manufactured by Oxford Instruments Asylum Research. The probes tested include ASYELEC.01-R2 and AC 160TS-R3 from Asylum Research, Multi75G and TAP300G from BudgetSensor, and AD-2.8-AS diamond probe from Adama Innovations.

Code Implementation

Botorch [36] was utilized as the Bayesian optimization framework, employing the Expected Improvement (EI) acquisition function. The surrogate Gaussian Process (GP) model was incorporated using gpytorch [37]. In the optimization of two scanning parameters described in this paper, we sampled the reward function in a parameter space with 100 x 100 pixels. All the parameters are normalized to be within (0, 1)

Acknowledgement

The development of automated workflow for SPM optimization (YL, SVK) was supported by the Center for Advanced Materials and Manufacturing (CAMM), the NSF MRSEC center. The combinatorial library growth (RE, PDR) was supported by the National Science Foundation

Materials Research Science and Engineering Center program through the UT Knoxville Center for Advanced Materials and Manufacturing (DMR-2309083). TiO₂ nanoparticles and CBI and MBI microparticles synthesis (A. D.) are supported by individual postdoctoral funding program German Academic Exchange Service (Deutscher Akademischer Austauschdienst: DAAD-PRIME2023). PTO (110) growth (JCY, YCL) acknowledged the financial support from National Science and Technology Council (NSTC) in Taiwan, under grant no. NSTC 112-2112-M-006-020-MY3. M.A. acknowledges support from the National Science Foundation, Award Number 2043205.

Supplementary Materials

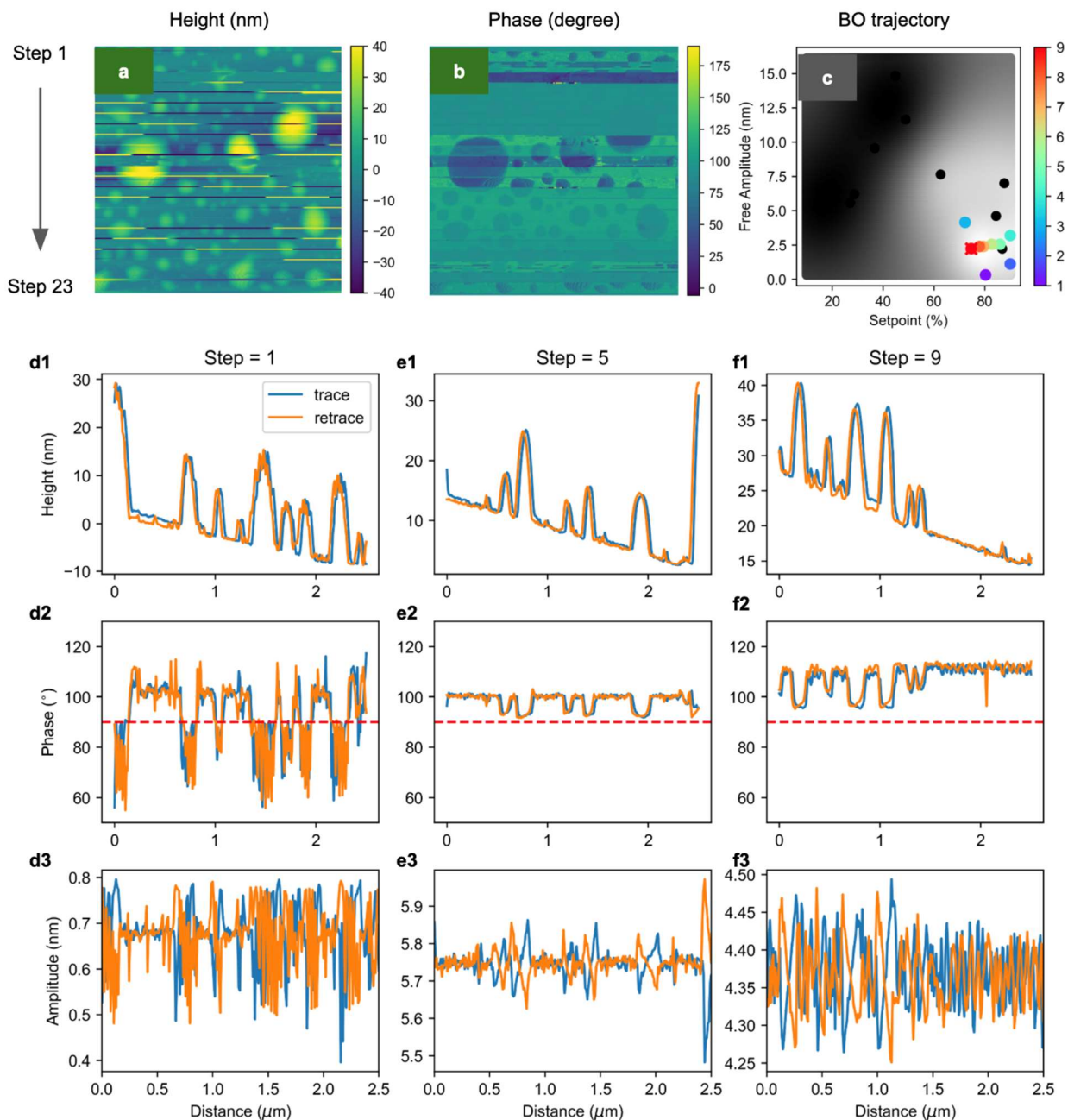


Figure S1. Visualization of the training process on water droplets. **a**, Topography map acquired on the droplet sample during the training process. In this map, each “jumping line” represents an update of scanning parameters and there are 23 steps in this single scan. After the scanning becomes stable, five subsequent trace and retrace scanning lines of height, phase and amplitude channels will be recorded to compute the reward function for currently used

parameters. **b**, corresponding phase map shows the evolution of phase angles during the training process. **c**, BO trajectory shows how the workflow explores the parameter space. **d1-d3**, the trace and retrace scanning lines of **d1** height, **d2** phase, and **d3** amplitude channels at step 1. Similar scanning lines for **e1-e3** step 5 and **f1-f3** step 9 are also plotted. The images taken with the optimized parameters are shown in the Figure 4.

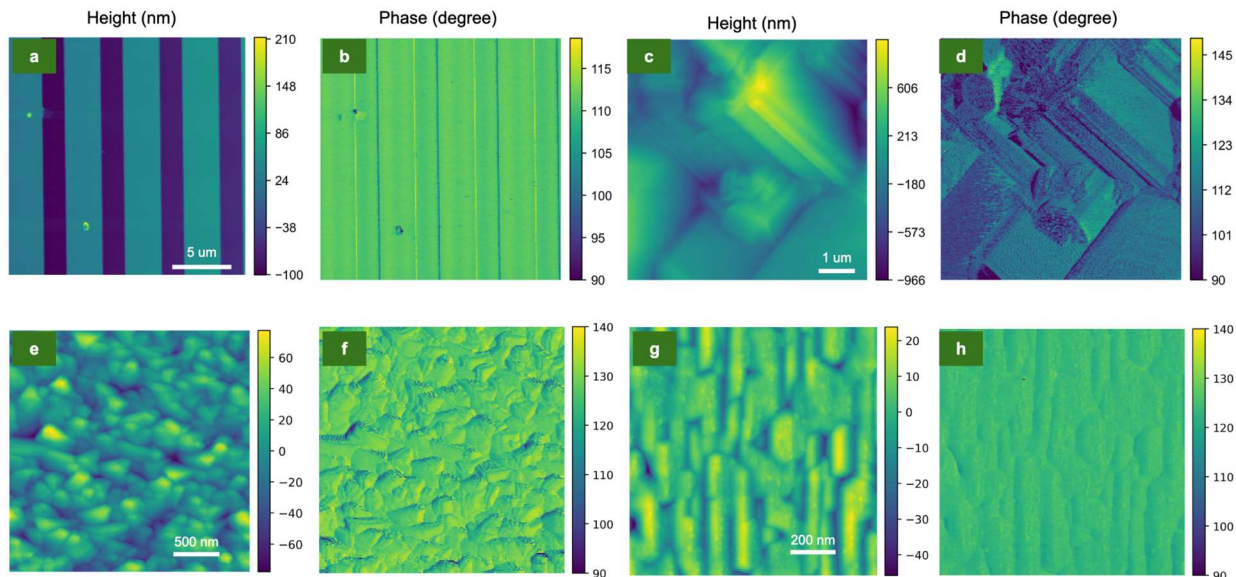


Figure S2. Testing the workflow on different samples. **a**, Topography map acquired with the optimized scanning parameters given by our automated workflow on height calibration grating sample from Asylum Research. **b**, corresponding phase map taken on the calibration grating sample. Similar maps acquired on **c-d** CBI nanoparticles **e-f** $(\text{CrVTaW})_x\text{Mo}_{1-x}$ alloy **g-h** PbTiO_3 ferroelectric thin-film.

I. Detailed analysis of BO exploration trajectories

Surprisingly, the BO exploration trajectory in Figure S1 shows that our autonomous workflow emulates how experienced human operators optimize a microscope: after a few random exploratory steps, BO explores the scanning parameters along a pathway from small free-air amplitude and a large setpoint amplitude at step 3 to decreased free-air amplitude and setpoint amplitude at step 9.

II. Universality of the optimization

To verify the universality of our reward-driven autonomous optimization workflow, we tested the same workflow over different probes and samples. Samples tested include height

calibration grating sample from Asylum Research, PbTiO₃, (CrVTaW)_xMo_{1-x}, CBI microparticles, TiO₂ nanoparticles, water droplets with CaCl₂ salt.

Topography maps in Figure S2 were taken with scanning parameters optimized by our autonomous workflow and showed that our workflow can give optimal parameters for a wide range of samples with different scanning sizes, sample roughness and sample hardness.

References

1. Bian, K., C. Gerber, A.J. Heinrich, D.J. Müller, S. Scheuring, and Y. Jiang, *Scanning probe microscopy*. Nature Reviews Methods Primers, 2021. **1**(1): p. 36.
2. Hansma, P.K., J.P. Cleveland, M. Radmacher, D.A. Walters, P.E. Hillner, M. Bezanilla, M. Fritz, D. Vie, H.G. Hansma, C.B. Prater, et al., *Tapping mode atomic force microscopy in liquids*. Applied Physics Letters, 1994. **64**(13): p. 1738-1740.
3. Drake, B., C.B. Prater, A.L. Weisenhorn, S.A.C. Gould, T.R. Albrecht, C.F. Quate, D.S. Cannell, H.G. Hansma, and P.K. Hansma, *Imaging Crystals, Polymers, and Processes in Water with the Atomic Force Microscope*. Science, 1989. **243**(4898): p. 1586-1589.
4. Binnig, G., C.F. Quate, and C. Gerber, *Atomic Force Microscope*. Physical Review Letters, 1986. **56**(9): p. 930-933.
5. Binnig, G., H. Rohrer, C. Gerber, and E. Weibel, *Surface Studies by Scanning Tunneling Microscopy*. Physical Review Letters, 1982. **49**(1): p. 57-61.
6. Sumaiya, S.A. and M.Z. Baykara, *Atomic-scale imaging and spectroscopy via scanning probe microscopy: An overview*. Journal of Vacuum Science & Technology B, 2023. **41**(6).
7. Bykov, I.V. *Automatized methods for optimization of scanning probe microscope operation*. in *2008 Third International Forum on Strategic Technologies*. 2008.
8. García, R. and A. San Paulo, *Attractive and repulsive tip-sample interaction regimes in tapping-mode atomic force microscopy*. Physical Review B, 1999. **60**(7): p. 4961-4967.
9. Herruzo, E.T., A.P. Perrino, and R. Garcia, *Fast nanomechanical spectroscopy of soft matter*. Nature Communications, 2014. **5**(1): p. 3126.
10. Tetard, L., A. Passian, S. Jung, A.J. Ragauskas, and B.H. Davison, *Development of New Methods in Scanning Probe Microscopy for Lignocellulosic Biomass Characterization*. Industrial Biotechnology, 2012. **8**(4): p. 245-249.
11. Martin, Y., C.C. Williams, and H.K. Wickramasinghe, *Atomic force microscope-force mapping and profiling on a sub 100-Å scale*. Journal of Applied Physics, 1987. **61**(10): p. 4723-4729.
12. Heinrich, A.J., J.A. Gupta, C.P. Lutz, and D.M. Eigler, *Single-Atom Spin-Flip Spectroscopy*. Science, 2004. **306**(5695): p. 466-469.
13. Dufrêne, Y.F., D. Martínez-Martín, I. Medalsy, D. Alsteens, and D.J. Müller, *Multiparametric imaging of biological systems by force-distance curve-based AFM*. Nature Methods, 2013. **10**(9): p. 847-854.

14. MARTI, O., V. Elings, M. Haugan, C.E. Bracker, J. Schneir, B. Drake, S.A.C. Gould, J. Gurley, L. Hellemans, K. Shaw, et al., *Scanning probe microscopy of biological samples and other surfaces*. Journal of Microscopy, 1988. **152**(3): p. 803-809.
15. Ozkan, A.D., A.E. Topal, F.B. Dikecoglu, M.O. Guler, A. Dana, and A.B. Tekinay, *Probe microscopy methods and applications in imaging of biological materials*. Seminars in Cell & Developmental Biology, 2018. **73**: p. 153-164.
16. Liu, Y., K.P. Kelley, R.K. Vasudevan, H. Funakubo, M.A. Ziatdinov, and S.V. Kalinin, *Experimental discovery of structure–property relationships in ferroelectric materials via active learning*. Nature Machine Intelligence, 2022. **4**(4): p. 341-350.
17. Crommie, M.F., C.P. Lutz, and D.M. Eigler, *Confinement of Electrons to Quantum Corrals on a Metal Surface*. Science, 1993. **262**(5131): p. 218-220.
18. Liu, Y., R. Proksch, C.Y. Wong, M. Ziatdinov, and S.V. Kalinin, *Disentangling Ferroelectric Wall Dynamics and Identification of Pinning Mechanisms via Deep Learning*. Advanced Materials, 2021. **33**(43): p. 2103680.
19. Loos, J., *The Art of SPM: Scanning Probe Microscopy in Materials Science*. Advanced Materials, 2005. **17**(15): p. 1821-1833.
20. Samorì, P., *Scanning probe microscopies beyond imaging*. Journal of Materials Chemistry, 2004. **14**(9): p. 1353-1366.
21. Sotres, J., H. Boyd, and J.F. Gonzalez-Martinez, *Enabling autonomous scanning probe microscopy imaging of single molecules with deep learning*. Nanoscale, 2021. **13**(20): p. 9193-9203.
22. Herminghaus, S., A. Fery, and D. Reim, *Imaging of droplets of aqueous solutions by tapping-mode scanning force microscopy*. Ultramicroscopy, 1997. **69**(3): p. 211-217.
23. McConney, M.E., S. Singamaneni, and V.V. Tsukruk, *Probing Soft Matter with the Atomic Force Microscopies: Imaging and Force Spectroscopy*. Polymer Reviews, 2010. **50**(3): p. 235-286.
24. Finlan, M.F. and I.A. McKay, U.S. Patent, 1990. **No. 5,047,633**.
25. Gleyzes, P., P.K. Kuo, and A.C. Boccaro, *Bistable behavior of a vibrating tip near a solid surface*. Applied Physics Letters, 1991. **58**: p. 2989-2991.
26. Ma, E.Y. and S. Simulator, *Scanning probe microscopy based on reinforcement learning*. 2015, Department of Applied Physics, Stanford University, California, United States.
27. Zhou, X., X. Dong, Y. Zhang, and Y. Fang. *Automatic tuning of PI controller for atomic force microscope based on relay with hysteresis*. in *2009 IEEE Control Applications,(CCA) & Intelligent Control,(ISIC)*. 2009. IEEE.
28. Ang, K.H., G. Chong, and Y. Li, *PID control system analysis, design, and technology*. IEEE transactions on control systems technology, 2005. **13**(4): p. 559-576.
29. O'Keefe, M.A., *"Resolution" in high-resolution electron microscopy*. Ultramicroscopy, 1992. **47**(1): p. 282-297.
30. Narasimha, G., S. Hus, A. Biswas, R. Vasudevan, and M. Ziatdinov, *Autonomous convergence of STM control parameters using Bayesian optimization*. APL Machine Learning, 2024. **2**(1).
31. Kalinin, S.V., S. Jesse, B.J. Rodriguez, J. Shin, A.P. Baddorf, H.N. Lee, A. Borisevich, and S.J. Pennycook, *Spatial resolution, information limit, and contrast transfer in piezoresponse force microscopy*. Nanotechnology, 2006. **17**(14): p. 3400.
32. Patil, S., N.F. Martinez, J.R. Lozano, and R. Garcia, *Force microscopy imaging of individual protein molecules with sub-pico Newton force sensitivity*. Journal of Molecular Recognition, 2007. **20**(6): p. 516-523.

33. Clayton, G.M., S. Tien, K.K. Leang, Q. Zou, and S. Devasia, *A Review of Feedforward Control Approaches in Nanopositioning for High-Speed SPM*. Journal of Dynamic Systems, Measurement, and Control, 2009. **131**(6).
34. Liu, Y., U. Pratiush, J. Bemis, R. Proksch, R. Emery, P.D. Rack, Y.-C. Liu, J.-C. Yang, S. Udovenko, S. Troler-McKinstry, et al. *Integration of Scanning Probe Microscope with High-Performance Computing: fixed-policy and reward-driven workflows implementation*. 2024. arXiv:2405.12300 DOI: 10.48550/arXiv.2405.12300.
35. Dubey, A., S.L. Sanchez, J. Yang, and M. Ahmadi, *Lead-Free Halide Perovskites for Photocatalysis via High-Throughput Exploration*. Chemistry of Materials, 2024. **36**(5): p. 2165-2176.
36. Balandat, M., B. Karrer, D.R. Jiang, S. Daulton, B. Letham, A.G. Wilson, and E. Bakshy *BoTorch: A Framework for Efficient Monte-Carlo Bayesian Optimization*. 2019. arXiv:1910.06403 DOI: 10.48550/arXiv.1910.06403.
37. Gardner, J.R., G. Pleiss, D. Bindel, K.Q. Weinberger, and A.G. Wilson *GPyTorch: Blackbox Matrix-Matrix Gaussian Process Inference with GPU Acceleration*. 2018. arXiv:1809.11165 DOI: 10.48550/arXiv.1809.11165.